DOI: 10.1002/cctc.200900243

Influence of Support Hydroxides on the Catalytic Activity of Oxidized Gold Clusters

Gabriel M. Veith,* Andrew R. Lupini, Stephen J. Pennycook, and Nancy J. Dudney[a]

Gold oxide nanoparticles were prepared on the native surface and a hydroxylated surface of a nonporous TiO_2 support (Degussa P25). Scanning transmission electron microscopy shows the formation of similarly sized clusters on both support materials (1.86 and 1.61 nm clusters on the native oxide and the hydroxylated oxide respectively). X-ray absorption near-edge spectroscopy and X-ray photoelectron spectroscopy clearly indicate the formation of Au^{3+}-rich oxide nanoparticles. Despite the similar cluster sizes and oxidation states, the gold oxide clusters grown on the hydroxylated surface were at least 180 times more catalytically active for the oxidation of carbon monoxide than those grown on the native oxide surface. Thus hydroxides, which are incidentally introduced during the solution-phase synthesis of gold catalysts, appear to play a dominant, but previously largely unrecognized, role in the catalytic properties of both oxidized and metallic gold particles.

Introduction

Hydroxy groups on the surface of oxide materials are known to influence the synthesis of supported metal catalysts.[1–3] Recent evidence suggests that they also influence the stability and activity of catalytic nanoparticles. Jensen et al. reported an increase in Cu cluster stability on hydroxylated Al_2O_3 surfaces up to 550 °C, compared to 450 °C for nonhydroxylated surfaces.[4] Amama et al. reported that Ostwald ripening of Fe catalysts on Al_2O_3 was inhibited during the growth of carbon nanotubes by hydroxy and oxygen species that reduced the Fe diffusion rate during growth conditions.[5] We recently reported that surface hydroxy groups, introduced during the solution-phase synthesis of supported gold clusters, were essential for stabilizing the gold clusters against coarsening under ambient conditions.[6] However, the precise role of the hydroxy groups remains an unresolved issue, as Hutchings and co-workers reported that surface hydroxy groups on FeOOH enhanced the coarsening of gold particles.[7]

In addition to increasing the metal cluster stabilities, we previously discovered that the activity of the gold clusters increased dramatically from $0.008\ mol_{CO}\,mol_{Au}^{-1}\,s^{-1}$ to $0.28\ mol_{CO}\,mol_{Au}^{-1}\,s^{-1}$ with the pH-dependent (acidic and basic) introduction of surface hydroxy groups to the TiO_2 surface.[6] This increase could not be attributed to the introduction of additional oxygen vacancies, changes in the support's surface area or pore structure, residual impurities, or differences in cluster sizes. Following our work demonstrating the dramatic effects of acid/base treatments on synthesis and reactivity of supported gold nanoparticles,[6] Edwards et al. verified these conclusions by reporting the formation of smaller catalyst particles and an enhancement towards the formation of H_2O_2 following a similar acid pretreatment of the same TiO_2.[8]

Another potentially important factor for catalytic activity is the oxidation state of the gold clusters. During the solution-phase synthesis of supported gold clusters oxidized gold species are trapped on the surface of the support material. These oxidized species are often reported to be, at least partly, responsible for the observed activity of supported gold catalysts.[9–16] Herein we report an investigation into the effect of a hydroxylated support material on an oxidized gold precursor. This work allows us to probe the effect of using an oxidized gold species and to determine whether the above-described effect of hydroxy groups is limited to metallic species or if it is applicable to oxidized gold species.

Results and Discussion

The results and discussion will focus on gold oxide nanoparticles grown on Degussa P25 support powder. This powder was used as-received (natural) or after the P25 was subjected to an aqueous-phase treatment at pH 10. The results presented below demonstrate that we were able to prepare gold oxide nanoparticles by reactive sputtering, and also that the particles are compositionally unstable and decomposed under ambient conditions over many months or with exposure to X-rays. There is a slight difference in weight loading for the two samples reported here (0.58 wt% AuO_x on natural TiO_2 and 0.49 wt% AuO_x on TiO_2 treated at pH 10) that is due to changes in the TiO_2 tamped density (mass/free packed volume) after aqueous phase processing.

[a] Dr. G. M. Veith, Dr. A. R. Lupini, Dr. S. J. Pennycook, Dr. N. J. Dudney
Materials Science and Technology Division, Oak Ridge National Laboratory
1 Bethel Valley Road, Oak Ridge, TN 37831 (USA)
Fax: (+1) 865-574-6210
E-mail: veithgm@ornl.gov

Supporting information for this article is available on the WWW under http://dx.doi.org/10.1002/cctc.200900243.

 © 2010 Wiley-VCH Verlag GmbH & Co. KGaA, Weinheim

Oxidation state of supported gold oxide clusters

Representative XPS data of the prepared AuO_x/TiO_2 catalysts (Figure 1) is consistent with the formation of an oxidized gold species. For the as-prepared samples, the main peak Au $4f_{7/2}$

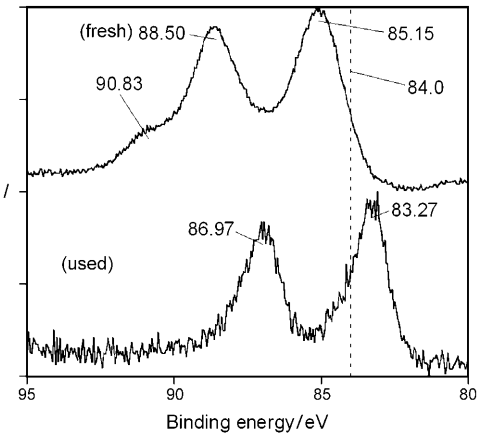

Figure 1. Normalized XPS data of fresh AuO_x on pH 10-treated TiO_2 (top) and AuO_x on pH 10-treated TiO_2 after it was used for the oxidation of CO (bottom). Dashed line indicates Au $4f_{7/2}$ binding energy of metallic gold foil.

peak has a binding energy of 85.15 eV, which is due to gold being oxidized.[17,18] For comparison, a metallic gold foil has an Au $4f_{7/2}$ binding energy of 84.0 eV (indicated by the dashed line in Figure 1). There is a second higher energy peak at 90.8 eV, which is consistent with the formation of an AuOH moiety (see the Supporting Information, S1).[17] There is no change in the O or Ti peak positions or shapes with the deposition of AuO_x. However, comparing the O and Ti XPS peak intensities for the gold oxide-coated and gold-free TiO_2 indicated a slightly higher O/Ti ratio for the AuO_x samples (1.17) than for the support (1.14). This slight increase in intensity is due to the extra oxygen present on the surface from the AuO_x. The O/Ti ratio returns to 1.14 upon reduction of the AuO_x. XPS compositional analysis from AuO_x films grown on Si and Al_2O_3 substrates indicates an O/Au atomic ratio of 55:45 with Mg X-rays and 65:35 with Zr x-rays thus indicating a AuO_x composition close to Au_2O_3.

Further evidence for the formation of gold oxides on the TiO_2 is presented in Figure 2, which shows the Au L_{III} XANES data for a catalyst sample along with several gold standards. A strong white line feature is observed for the AuO_x/TiO_2 sample, as well as the $AuCl_3$ and Au_2O_3 reference materials, originating from a spin-allowed 2p to 5d transition that occurs due to empty d orbitals present in oxidized gold samples.[19] As noted by Fierro-Gonzalez et al., the reduction in intensity of the white line is not a direct measurement of oxidation state, as illustrated by the differences in intensity for Au_2O_3 and $AuCl_3$, since the intensity is influenced by the coordinating ligands around the gold.[10] The intensity of this white line feature rapidly reduced with beam exposure due to the reduction of Au by the X-rays making it difficult to perform EXAFS analysis on

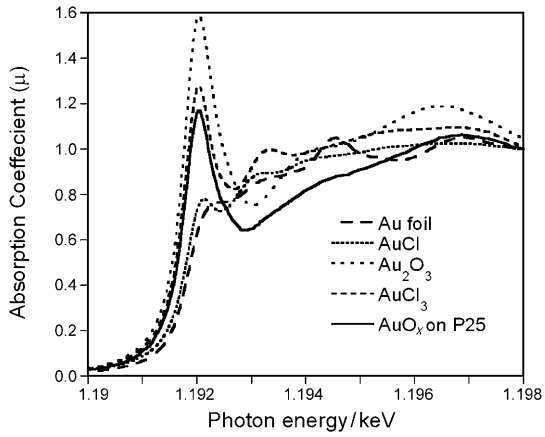

Figure 2. Au L_{III} XANES data for AuO_x on natural TiO_2, alongside $AuCl_3$, Au_2O_3, AuCl and Au foil reference spectra.

these materials (see the Supporting Information, S2). However, it can be concluded from the XPS and XANES data that the gold species are highly oxidized, close to Au^{3+}, but their exact structure is not known.

Structure of supported gold oxide catalysts

Representative STEM images for the AuO_x/natural TiO_2 and AuO_x/pH 10 TiO_2 are shown in Figures 3 and 4 respectively, and gold oxide nanoparticle histograms, derived from the STEM data, are presented in Figure 5. This data shows the formation

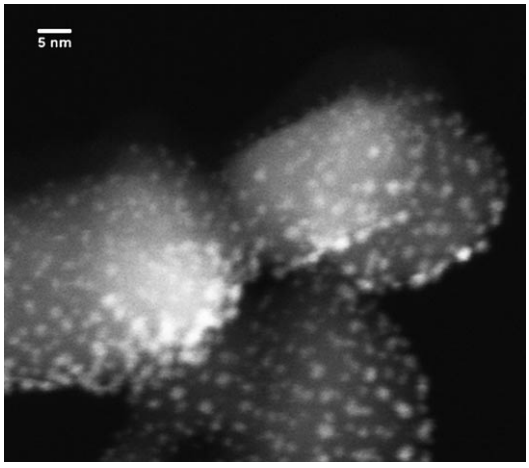

Figure 3. STEM image of as-prepared AuO_x on natural TiO_2. Gold oxide nanoparticles show up as bright white spots.

of gold oxide nanoparticles (bright white spots) with a narrow size variation on the surface of the TiO_2. Furthermore, the average nanoparticle size is virtually the same for the AuO_x clusters grown on natural P25 (1.86 nm) and pH 10-treated P25 (1.61 nm) with the slight reduction in average diameter of AuO_x/pH 10 TiO_2 due to the formation of very small catalyst

 © 2010 Wiley-VCH Verlag GmbH & Co. KGaA, Weinheim

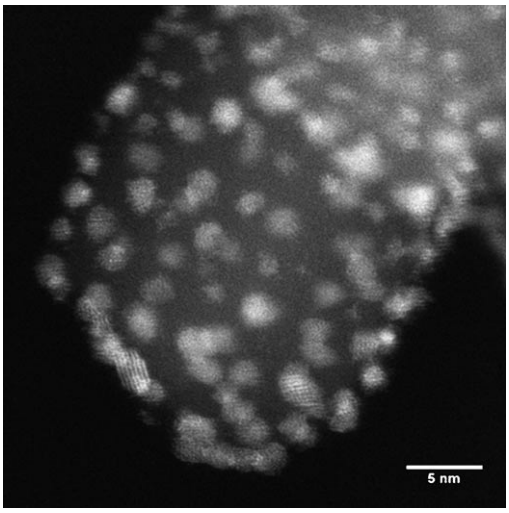

Figure 4. STEM image of as-prepared AuO_x on pH 10-treated TiO_2. Gold oxide nanoparticles show up as bright white spots.

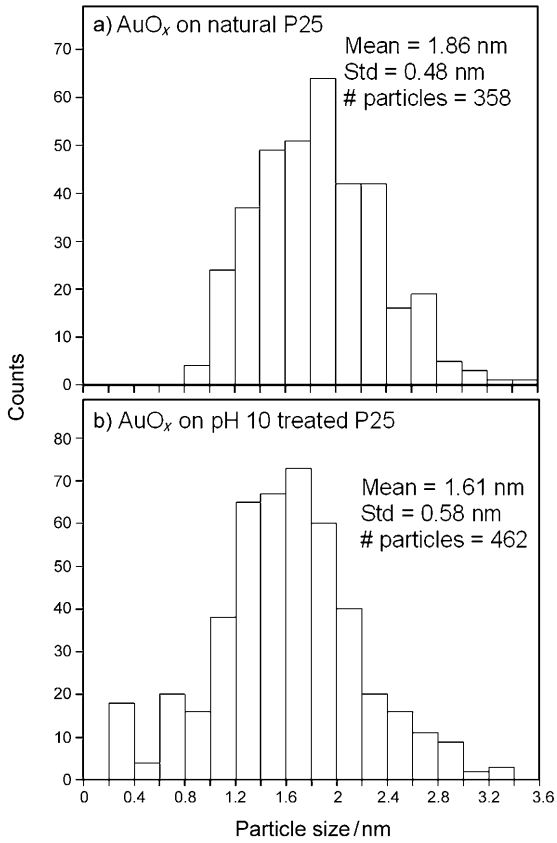

Figure 5. a) Particle-size histograms of as-prepared AuO_x on natural TiO_2; b) particle size histograms of as-prepared AuO_x on pH 10-treated TiO_2.

clusters (<0.8 nm; 9% total clusters) that are not seen for the AuO_x/natural TiO_2 samples. The formation of smaller particles on base-treated TiO_2 was detected for metallic gold nanoparticles and is attributed to the formation of more nucleation sites, which trap the incoming adatoms more efficiently.

Catalytic activity

Figure 6 shows a plot of activity for the oxidation of carbon monoxide ($mol_{CO}\,mol_{Au}^{-1}\,s^{-1}$) as a function of time for the oxidized gold clusters supported on the treated and natural TiO_2.

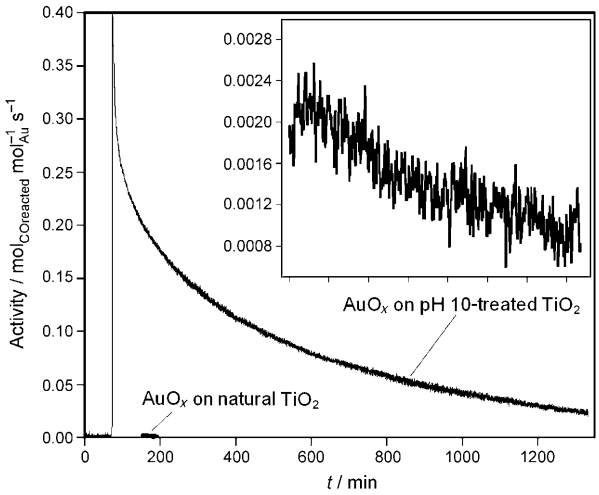

Figure 6. Room temperature catalytic activity data versus time for AuO_x nanoparticles supported on pH 10-treated TiO_2 and natural TiO_2. Note: The AuO_x/natural TiO_2 data has been artificially shifted to a higher time for clarity. Inset: Expanded view of AuO_x/natural TiO_2 data.

Activity measurements were performed such that less than 10% of the CO was converted to CO_2, to avoid working in the diffusion limiting regime and avoid "lighting off", from the exothermic decomposition of CO, which increases the temperature of the catalyst bed preventing direct comparisons. Catalysts with low weight loadings were investigated to further reduce the activity of the sample to obtain meaningful reaction rates; higher weight loadings were investigated but they were too active (AuO_x/pH 10 TiO_2). Due to the low activity of AuO_x/natural TiO_2, a space velocity of 10380 h^{-1} was used to get a measurable activity compared to a space velocity of 120000 h^{-1} for the catalysts grown on base treated P25. The initial activity of the gold oxide grown on pH 10-treated TiO_2 is around 180 times higher than that for Au/natural TiO_2 (0.4 vs. ca. 0.0022 $mol_{CO}\,mol_{Au}^{-1}\,s^{-1}$). However, this difference should be viewed as a lower limit due the large differences in space velocities used for these samples.

In both cases, there is a decrease in activity with time on stream. However, there is still significant activity of the sample grown on base-treated P25 after 20 h. Post-reaction analysis of the deactivated samples using XPS indicated that a reduction of Au occurred during the reaction (Figure 1). The gold binding energy shifted to about 83.3 eV from 85.15 eV.

Care should be taken when interpreting the binding energy shifts for small nanoparticles due to initial and final state effects.[20] The binding energy of the used sample was lower than that of bulk Au^0 but it was consistent with a reduced binding energy for supported metallic gold nanoparticles.[21–24] Further comparison of the XPS data shows an increase in the

 © 2010 Wiley-VCH Verlag GmbH & Co. KGaA, Weinheim

Ti/Au ratio (>10) for the deactivated reduced catalyst relative to the unreacted AuO_x (4.5) sample. An increase in the Ti/Au ratio indicates that a coarsening of the gold particles has occurred, thus exposing more of the surface Ti for analysis as the gold is trapped within larger particles and is no longer detected in the XPS.[6] However, these changes should be used as a guide, since the XPS measurement of the surface gold concentration in the gold oxide is reduced by the presence of the oxygen coordinated to the gold, which increases the Ti/Au ratio. STEM data showing the larger reduced particles is presented in Figure S3 (see the Supporting Information). This data shows that oxidized gold clusters can be highly catalytically active compared to metallic clusters on similar supports (0.28 $mol_{CO}\,mol_{Au}^{-1}\,s^{-1}$).[6] However, the instability of gold oxide effects the lifespan of the catalyst. The potential loss of hydroxy groups during the reaction is not considered a major source of deactivation because metallic gold clusters on hydroxylated TiO_2, unlike oxidized gold clusters, remain active and stable over many hours under reaction conditions.[6]

Pretreating the TiO_2 to an alkaline wash before growing the gold oxide nanoparticles resulted in a significant increase in catalytic activity. We have previously reported a similar, but not as large, increase in catalytic activity for metallic gold particles deposited on pH 10-treated TiO_2.[6] Pretreating the TiO_2 results in the formation of strongly bound surface hydroxy groups as indicated by FTIR spectroscopy of the catalysts. The new hydroxy groups, detected on the base-treated TiO_2, have an OH vibrational frequency at a higher wavenumber, (3439 cm^{-1}) than that for the as-received P25 (3345 cm^{-1}).[6] This higher frequency OH band corresponds to OH groups bound to Ti, whereas the lower frequency band corresponds to molecular water adsorbed on the surface of the TiO_2 from the air.[25–29] Other characterization methods such as gas physisorption, XPS, and XRD showed no measurable changes in the support material with treatment.[6] XPS results showed that there was no Na or Cl impurity after the base/washing treatment (see the Supporting Information, Figure S4).

The introduction of a strongly bound surface hydroxy species during the solution-phase processing of the TiO_2 resulted in an enhancement in catalytic activity through one of two plausible mechanisms. Firstly, the surface hydroxy groups could participate in the reaction by helping to stabilize an intermediate state or activating a reactant. Secondly, the presence of surface hydroxy groups could facilitate the formation of small nanoparticles through the creation of nucleation/trapping sites to stabilize the smaller (<0.8 nm) gold oxide clusters, which may be more catalytically active.[7]

Herzing et al. attributed the activity of gold catalysts supported on $FeOOH/Fe_2O_3$ to the formation of approximately 0.5 nm bilayer clusters of about ten gold atoms.[7] The initial gold clusters reported by Herzing et al. were oxidized, as evidenced by a gold XPS binding energy of 85.1 eV,[7] similar to the catalysts prepared in this work. Upon annealing, their gold clusters were reduced to Au^0 and there was a loss of activity that was attributed to the loss of the bilayer clusters.[7]

Microscopy data collected for our samples show the formation of some smaller gold clusters (<0.8 nm, about 9% of the total clusters) on the hydroxylated support material that are not observed for the gold catalysts on the untreated oxide. Furthermore, only about 1% of the total clusters are in the 0.5 nm size range. Using the results of Herzing et al.[7] and Valden et al., [30] we might expect that these particles should be the most active catalysts. However, we do not believe the increase in activity is due to the formation of smaller gold clusters for the following reasons. Firstly the support materials used by those authors[7,30] differ substantially from those in the present work ($FeOOH/Fe_2O_3$ vs. TiO_2 films vs. TiO_2 powders). The type of support is known to have a dramatic influence on the catalytic properties,[31] so it is not certain whether we should expect the same mechanism to apply. Secondly, microscopy and activity studies, by use of the World Gold Council reference Au/TiO_2 catalyst, shows 3.7 nm gold clusters (none smaller than 1.5 nm) along with a comparable, more stable, activity (0.3 $mol_{CO}\,mol_{Au}^{-1}\,s^{-1}$) than our AuO_x/pH 10 TiO_2 catalysts despite having a larger average gold cluster size.[32]

These results strongly support a mechanism, reported by us and others, whereby hydroxy groups[6,33–37] or water[33,34,38–42] play a role in the catalytic oxidation of carbon monoxide. The results of this study do not settle the controversy of whether the active species in supported gold catalysts is an oxidized gold or metallic gold component. However, these results and those from our previous work[6] clearly demonstrate that the convenient introduction of surface hydroxy groups to the surface of TiO_2 during solution-phase processing leads to the formation of both smaller gold (oxidized and metallic) nanoparticles along with a significant increase in catalytic activity over catalysts supported on nonhydroxylated supports (36-fold for metallic gold nanoparticles in our previous work and 180-fold for oxidized gold nanoparticles in this study).

Conclusions

By using the reactive sputtering technique of magnetron sputtering, we were able to prepare supported gold oxide nanoparticles on TiO_2, both on a native TiO_2 surface and on TiO_2 that had been treated in solution to hydroxylate the surface. This data shows that simply having an oxidized gold catalyst does lead to some catalytic activity (2×10^{-3} $mol_{CO}\,mol_{Au}^{-1}\,s^{-1}$). However, the critical parameters to the formation of highly active gold catalysts is the presence of the hydroxy groups during the synthesis of supported gold catalysts. Without surface hydroxy groups, the oxidized gold clusters are poorly active towards the oxidation of CO, but with the surface hydroxy groups there is a 180-fold increase in activity.

Experimental Section

Rather than using traditional solution-phase synthesis techniques, such as impregnation, incipient wetness, or precipitation, we employed a physical vapor deposition process to deposit metal atoms onto bulk support materials where they nucleated and grew to form catalytic nanoparticles.[32,43–45] This process enabled us to deposit metal nanoparticles on the native oxide surface (i.e. a surface that hadn't been modified by the solution-phase synthesis of sup-

 © 2010 Wiley-VCH Verlag GmbH & Co. KGaA, Weinheim

ported metal nanoparticles).[32,43–45] In addition we could treat the support material using a mock-solution-phase synthesis procedure whereby the same synthesis conditions used traditionally to prepare supported metal nanoparticles (i.e. pH, temperatures, ion species, filtering), were performed on the support material in the absence of metal precursors, followed by vapor deposition of metal clusters on the support surface.[6] Understanding the differences in materials properties allowed us to begin to understand how the synthetic methods influenced the resulting catalytic properties.

Most of the procedures used in this paper were described previously[6] so only brief procedural highlights will be presented along with experimental differences. Degussa P25 (fine powder, 5 g) was added to ultrapure deionized water (400 mL, 18.3 MΩ) and vigorously stirred to simulate the commonly used deposition–precipitation (DP) technique. Degussa P25 was used for this study because when it is prepared, by the flame hydrolysis of $TiCl_4$, it results in the production of nonporous TiO_2 that has not been exposed to solution processing. The P25/H_2O mixture was adjusted to pH 10 by the stepwise addition of 0.2 M NaOH (97%, ACS Grade, Alfa Aesar). The solution was heated to 57 °C and maintained at this temperature for 2 h. The pH was actively controlled at the elevated temperature by adding NaOH to keep the pH constant, as it tended to decrease over time. Approximately 5×10^{-3} mol of Cl^- was added to the pH 10 mixture by the dropwise addition of 0.1 M HCl to simulate the presence of Cl^- from the auric acid in conventional DP synthesis. The warm mixtures were centrifuged and washed to collect the powders, but only about 75% of the P25 could be centrifuged out of solution and collected. The collected powder was dried for 20 h in a vacuum oven at room temperature and stored in a $CaSO_4$-filled desiccator prior to use. The resulting powder has the same X-ray photoelectron spectrum, powder X-ray diffraction (XRD) pattern, and Fourier transform infrared spectrum (FTIR) as reported previously.[6]

Catalyst preparation entailed placing the native or pH 10-treated titania (ca. 1 g) and two one-inch Teflon-coated stir bars inside a set of stainless steel cups attached to a vacuum-compatible motor. A high-purity gold target (Refining Systems, Inc. Nevada USA, 99.995%) was reactively sputtered for 60 min, at an applied power of 50 W, by direct current (dc) magnetron sputtering in an O_2 atmosphere (Research Grade, UHP Grade - Air Liquide). The stainless steel cups were rotated causing the powders to tumble constantly, exposing new regions of the titania for the sputtered gold to deposit onto. Under these deposition conditions, substrates had to be at least 7 cm away from the gold target; closer than 7 cm and the gold would not oxidize resulting in the formation of Au^0 nanoparticles. Gold loading was determined by using a Thermo Jarrell Ash IRIS inductively coupled plasma (ICP) optical emission spectrometer.[6] Gold loadings varied, from 0.58 wt% for AuO_x/natural TiO_2 to 0.49 wt% for AuO_x/pH 10 TiO_2, due to differences in the support's volume.[6] The resulting gold oxide nanoparticles supported on TiO_2 support material had an off-white color (see the Supporting Information, S5).

For additional characterization studies, gold oxide films were simultaneously grown on thin glass slides, Al_2O_3 substrates (Coors), and [100] aligned Si wafers located next to the rotating drum at the same height as the powders. Gold oxide films were also grown as part of this study to compare with previous reports in the literature for the vapor formation of Au_2O_3.[17,46–48] Films of AuO_x grown on Al_2O_3 substrates had a black color (see the Supporting Information, S5) and were stable for over two weeks. After this time, visible degradation of the film and powders was observed, producing a clear change in color (see the Supporting Information, S5). Temperature-programmed decomposition reactions showed that the gold oxide decomposed starting at 227 °C to Au^0 (see the Supporting Information, S6). The XRD and FTIR data (see the Supporting Information, S7 and S8) of the AuO_x films are consistent with previously reported data for the formation of Au_2O_3 films.[47]

X-ray absorption near-edge spectroscopy (XANES) data were collected at the National Synchrotron Light Source at Brookhaven National Laboratory on beamline X19A in both transmission and fluorescence mode and compared to reference gold foil for precise energy calibration. Sample and gold references (Au, AuCl, $AuCl_3$, and Au_2O_3, all >99.9%, Alfa Aesar) were pressed into a copper sample holder and held in place with Kapton tape. Data reduction and analysis was performed with the Athena/Artemis suite of programs.[49]

XPS data were collected using a PHI 3056 spectrometer with a Mg/Zr anode source operated at 15 kV and an applied power of 350 W. Samples were manually pressed between two pieces of indium foil; the piece of In foil with the sample on it was then mounted to the sample holder with a piece of carbon tape (Nisshin E. M. Co. Ltd). Indium was used as a support since the C 1s binding energy, from adventitious carbon, was used to calibrate the binding energy shifts of the sample (C 1s = 284.5 eV).[50] High-resolution data were collected with a pass energy of 5.85 eV with 0.05 eV step sizes and a minimum of 200 scans to improve the signal to noise ratio; lower resolution survey scans were collected at a pass energy of 93.5 eV with 0.5 eV step sizes and a minimum of 25 scans. Raw gold XPS data is presented in the Supporting Information, S9; Survey data from the TiO_2 is shown in the Supporting Information, S4, with the inset showing the region where Na would appear if present.

High-angle annular dark field (HAADF) imaging was performed to image the AuO_x particles on a VG Microscopes HB603 UHV scanning transmission electron microscope (STEM), with a resolution better than 0.8 Å,[51] operating at 300 kV and equipped with an aberration corrector from Nion Co. and also on a Hitachi HD2000 STEM operating at 200 kV.

The room temperature (24 °C) catalytic activity of the AuO_x/TiO_2 catalysts was determined by using a custom-built flow reactor to monitor the conversion of carbon monoxide to carbon dioxide. Powders of AuO_x/natural TiO_2 (0.04 g) or AuO_x/pH 10 TiO_2 (ca. 0.01 g) catalyst were loaded into a quartz U-tube (i.d. = 4 mm) and supported on both ends with glass wool. A mixture of high purity Helium (99.99%, Air Liquide), oxygen (ultrahigh purity, Air Liquide), and carbon monoxide (research grade, Matheson, stored in an aluminum cylinder) was delivered from three Sierra Instruments Mass Flow valves at rates of 45, 6, and 2 sccm, respectively. The product evolution was monitored with an Ametek Dymaxion mass spectrometer (0–200 amu range). The temperature of the catalyst bed was determined using an embedded K-type thermocouple.

Acknowledgements

The authors thank Degussa for donating the P25 and Nebojsa (Ned) Marinkovic for helping with the XANES measurements. Microscopy studies at Oak Ridge National Laboratory's Center for Nanophase Materials Sciences, were sponsored by the Scientific User Facilities Division, Office of Basic Energy Sciences, U.S. Department of Energy. Use of the National Synchrotron Light

 © 2010 Wiley-VCH Verlag GmbH & Co. KGaA, Weinheim

Source, Brookhaven National Laboratory, was supported by the U.S. Department of Energy, Office of Science, Office of Basic Energy Sciences, under Contract No. DE-AC02-98CH10886. This research was sponsored by the Division of Materials Sciences and Engineering, U.S. Department of Energy under contract with UT-Battelle, LLC.

Keywords: gold · heterogeneous catalysis · hydroxylation · oxidation · supported catalysts

[1] M. Hisamoto, R. C. Nelson, M.-Y. Lee, J. Eckert, S. L. Scott, *J. Phys. Chem. C* **2009**, *113*, 8794 – 8805.
[2] L. Jiao, J. R. Regalbuto, *J. Catal.* **2008**, *260*, 329 – 341.
[3] K. Bourikas, C. Kordulis, A. Lycourghiotis, *Catal. Rev.* **2006**, *48*, 363 – 444.
[4] M. C. R. Jensen, K. Venkataramani, S. Helveg, B. S. Clausen, M. Reichling, F. Besenbacher, J. V. Lauritsen, *J. Phys. Chem. C* **2008**, *112*, 16953 – 16960.
[5] P. B. Amama, C. L. Pint, L. McJilton, S. M. Kim, E. A. Stach, P. T. Murray, R. H. Hauge, B. Maruyama, *Nano Lett.* **2009**, *9*, 44 – 49.
[6] G. M. Veith, A. R. Lupini, N. J. Dudney, *J. Phys. Chem. C* **2009**, *113*, 269 – 281.
[7] A. A. Herzing, C. J. Kiely, A. F. Carley, P. Landon, G. J. Hutchings, *Science* **2008**, *321*, 1331 – 1335.
[8] J. K. Edwards, E. Ntainjua N, A. F. Carley, A. A. Herzing, C. J. Kiely, G. J. Hutchings, *Angew. Chem.* **2009**, *121*, 8664 – 8667; *Angew. Chem. Int. Ed.* **2009**, *48*, 8512 – 8515.
[9] L. Fu, N. Q. Wu, J. H. Yang, F. Qu, D. L. Johnson, M. C. Kung, H. H. Kung, V. P. Dravid, *J. Phys. Chem. B* **2005**, *109*, 3704 – 3706.
[10] J. C. Fierro-Gonzalez, B. C. Gates, *Catal. Today* **2007**, *122*, 201 – 210.
[11] Q. Fu, H. Saltsburg, M. Flytzani-Stephanopoulos, *Science* **2003**, *301*, 935 – 938.
[12] C. K. Costello, J. Guzman, J. H. Yang, Y. M. Wang, M. C. Kung, B. C. Gates, H. H. Kung, *J. Phys. Chem. B* **2004**, *108*, 12529 – 12536.
[13] M. Ferrandon, T. Krause, *Appl. Catal. A* **2006**, *311*, 135 – 145.
[14] A. Karpenko, R. Leppelt, V. Plzak, R. J. Behm, *J. Catal.* **2007**, *252*, 231 – 242.
[15] M. Mihaylov, B. C. Gates, J. C. Fierro-Gonzalez, K. Hadjiivanov, H. Knözinger, *J. Phys. Chem. C* **2007**, *111*, 2548 – 2556.
[16] M. Mihaylov, E. Ivanova, Y. Hao, K. Hadjiivanov, H. Knözinger, B. C. Gates, *J. Phys. Chem. C* **2008**, *112*, 18973 – 18983.
[17] T. Dickinson, A. F. Povey, P. M. A. Sherwood, *J. Chem. Soc. Faraday Trans. 1* **1975**, *71*, 298 – 311.
[18] L. K. Ono, B. Roldan Cuenya, *J. Phys. Chem. C* **2008**, *112*, 4676 – 4686.
[19] J. W. Watkins, II, R. C. Elder, B. Greene, D. W. Darnall, *Inorg. Chem.* **1987**, *26*, 1147 – 1151.
[20] R. Meyer, C. Lemire, S. K. Shaikhutdinov, H.-J. Freund, *Gold Bull.* **2004**, *37*, 72 – 124.
[21] J. Radnik, C. Mohr, P. Claus, *Phys. Chem. Chem. Phys.* **2003**, *5*, 172 – 177.
[22] M. P. Casaletto, A. Longo, A. Martorana, A. Prestianni, A. M. Venezia, *Surf. Interface Anal.* **2006**, *38*, 215 – 218.
[23] S. Arrii, F. Morfin, A. J. Renouprez, J. L. Rousset, *J. Am. Chem. Soc.* **2004**, *126*, 1199 – 1205.
[24] A. Zwijnenburg, A. Goossens, W. G. Sloof, M. W. J. Crajé, A. M. van der Kraan, L. J. de Jongh, M. Makkee, J. A. Moulijn, *J. Phys. Chem. B* **2002**, *106*, 9853 – 9862.
[25] Z. Ding, G. Q. Lu, P. F. Greenfield, *J. Phys. Chem. B* **2000**, *104*, 4815 – 4820.
[26] L. Wu, J. C. Yu, L. Zhang, X. Wang, W. Ho, *J. Solid State Chem.* **2004**, *177*, 2584 – 2590.
[27] B. Erdem, R. A. Hunsicker, G. W. Simmons, E. D. Sudol, V. L. Dimonie, M. S. El-Aasser, *Langmuir* **2001**, *17*, 2664 – 2669.
[28] Y. Suda, T. Morimoto, *Langmuir* **1987**, *3*, 786 – 788.
[29] K. Tanaka, J. M. White, *J. Phys. Chem.* **1982**, *86*, 4708 – 4714.
[30] M. Valden, X. Lai, D. W. Goodman, *Science* **1998**, *281*, 1647 – 1650.
[31] M. M. Schubert, S. Hackenberg, A. C. van Veen, M. Muhler, V. Plzak, R. J. Behm, *J. Catal.* **2001**, *197*, 113 – 122.
[32] G. M. Veith, A. R. Lupini, S. N. Rashkeev, S. J. Pennycook, D. R. Mullins, V. Schwartz, C. A. Bridges, N. J. Dudney, *J. Catal.* **2009**, *262*, 92 – 101.
[33] C. K. Costello, M. C. Kung, H.-S. Oh, Y. Wang, H. H. Kung, *Appl. Catal. A: Gen* **2002**, *232*, 159 – 168.
[34] H. H. Kung, M. C. Kung, C. K. Costello, *J. Catal.* **2003**, *216*, 425 – 432.
[35] V. Aguilar-Guerrero, R. J. Lobo-Lapidus, B. C. Gates, *J. Phys. Chem. C* **2009**, *113*, 3259 – 3269.
[36] F. Moreau, G. C. Bond, B. van der Linden, B. A. A. Silberova, M. Makkee, *Appl. Catal. A* **2008**, *347*, 208 – 215.
[37] H. Zhu, Z. Ma, J. C. Clark, Z. Pan, S. H. Overbury, S. Dai, *Appl. Catal. A* **2007**, *326*, 89 – 99.
[38] M. Daté, Y. Ichihashi, T. Yamashita, A. Chiorino, F. Boccuzzi, M. Haruta, *Catal. Today* **2002**, *72*, 89 – 94.
[39] M. Daté, M. Okumura, S. Tsubota, M. Haruta, *Angew. Chem.* **2004**, *116*, 2181 – 2184; *Angew. Chem. Int. Ed.* **2004**, *43*, 2129 – 2132.
[40] M. C. Kung, R. J. Davis, H. H. Kung, *J. Phys. Chem. C* **2007**, *111*, 11767 – 11775.
[41] J. T. Calla, R. J. Davis, *J. Catal.* **2006**, *241*, 407 – 416.
[42] M. A. Debeila, R. P. K. Wells, J. A. Anderson, *J. Catal.* **2006**, *239*, 162 – 172.
[43] G. M. Veith, A. R. Lupini, S. J. Pennycook, N. J. Dudney in *Studies in Surf. Sci. and Catalysis*, 162 (Eds.: E. Gaigneaux, M. Devillers, D. E. De Vos, S. Hermans, P. A. Jacobs, J. A. Martens, P. Ruiz), Elsevier, Amsterdam, pp. 71 – 78.
[44] G. M. Veith, A. R. Lupini, S. J. Pennycook, G. W. Ownby, N. J. Dudney, *J. Catal.* **2005**, *231*, 151 – 158.
[45] G. M. Veith, A. R. Lupini, S. J. Pennycook, A. Villa, L. Prati, N. J. Dudney, *Catal. Today* **2007**, *122*, 248 – 253.
[46] A. M. Klumb, C. R. Aita, N. C. Tran, *J. Vac. Sci. Technol. A* **1989**, *7*, 1697 – 1701.
[47] L. Maya, M. Paranthaman, T. Thundat, M. L. Bauer, *J. Vac. Sci. Technol. B* **1996**, *14*, 15 – 21.
[48] H. Shi, R. Asahi, C. Stampfl, *Phys. Rev. B* **2007**, *75*, 205125.
[49] B. Ravela, M. Newville, *J. Synchrotron Radiat.* **2005**, *12*, 537 – 541.
[50] J. F. Moulder, W. F. Stickle, P. E. Sobol, K. D. Bomben, *Handbook of X-ray Photoelectron Spectroscopy*, Perkin–Elmer Corp., **1992**.
[51] P. D. Nellist, M. F. Chisholm, N. Dellby, O. L. Krivanek, M. F. Murfitt, Z. S. Szilagyi, A. R. Lupini, A. Borisevich, W. H. Sides Jr., S. J. Pennycook, *Science* **2004**, *305*, 1741.

Received: September 23, 2009
Published online on January 5, 2010

 © 2010 Wiley-VCH Verlag GmbH & Co. KGaA, Weinheim